Substrate Modifications for Stability Improvements of Flexible Perovskite Solar Cells

Jingyang Lin, Yanling He, Hongbo Mo, Abdul Khaleed, Zhilin Ren, Yin Li, Yingnan Cao, Jinyao Tang, Wei-Ting Wang, Shien-Ping Feng, Zhao Sun, Wen-Di Li, Tao Zhu, Gang Li, Alan Man Ching Ng,* and Aleksandra B. Djurišić*

Flexible perovskite solar cells (fPSCs) prepared on flexible plastic substrates exhibit poor stability under illumination in ambient, due to inferior gas barrier properties of plastic substrates. Herein, we investigated effect of different modifications of the back surface of the substrate to improve stability under illumination in ambient. T_{80} under simulated solar illumination at maximum power point in ambient (ISOS-L-1) can be increased from 80 h to over 350 h with the deposition of a single layer (by spin-coating or by atomic layer deposition (ALD)). While ALD layers resulted in the best T_{80} value and significant reduction of the oxygen transmission rate compared to other modifications even for very low film thickness ($\approx$10 nm), a simple solution-processed spin-on-glass barrier layer also enables significant (more than 4 times) improvement in device stability. This work illustrates the importance of barrier layers for decreasing the ingress of oxygen and moisture into fPSCs through the plastic substrate.

1. Introduction

Flexible perovskite solar cells (fPSCs)[1–48] are of significant interest due to their high power-per-weight ratios, potential for low cost fabrication on inexpensive flexible substrates, such as roll-to-roll (R2R) manufacturing, and the rising demand for niche applications of solar power (vehicle integrated photovoltaics, space applications, Internet of Things (IoT), wearable electronics, etc.).[1–3,5,6,9] A significant obstacle toward commercialization fPSCs, among others, is their lower efficiency and stability compared to rigid devices.[1,5] In recent years, significant progress has been made in improving the efficiency of fPSCs, with power conversion efficiency (PCE) of small single-junction devices exceeding 21–22%,[7,9,10,25–27,31,41] and record efficiency of a flexible tandem device of 24.7%.[10,31,43] High efficiencies have been achieved in both conventional and inverted architectures, and commonly involve optimization of charge transport layers, the use of additives and/or interface/grain boundary passivations.[2,3,7] These strategies are also expected to improve the device stability. However, the improvements in stability of fPSCs, in particular operational stability, are lagging behind those of rigid devices more significantly compared to improvements in other performance parameters.

Stability considerations of fPSCs typically take into account mechanical stability and environmental stability.[2] Consequently, mechanical stability investigations of fPSCs[2,14,15,17–22,24–28,32–34,36,37,44–48] and environmental stability in ambient without illumination have been very common.[2,14–21,24,26,28,32,33,36–39,44,46–48] Impressive improvements have been achieved in mechanical stability, with reports

J. Lin, Y. He, H. Mo, A. Khaleed, Z. Ren, Y. Li, A. B. Djurišić
Department of Physics
University of Hong Kong
Pokfulam Road, Hong Kong, Hong Kong
E-mail: dalek@hku.hk

J. Lin, A. M. C. Ng
Department of Physics and Core Research Facilities
Southern University of Science and Technology
No. 1088, Xueyuan Rd., Shenzhen, Guangdong 518055, P. R. China
E-mail: ngamc@sustech.edu.cn

The ORCID identification number(s) for the author(s) of this article can be found under https://doi.org/10.1002/ente.202300958.

Y. Cao, J. Tang
Department of Chemistry
University of Hong Kong
Pokfulam Road, Hong Kong, Hong Kong

W.-T. Wang, S.-P. Feng
Department of Systems Engineering
City University of Hong Kong
Kowloon, Hong Kong

Z. Sun, W.-D. Li
Department of Mechanical Engineering
University of Hong Kong
Pokfulam Road, Hong Kong, Hong Kong

T. Zhu, G. Li
Department of Electrical and Electronic Engineering
Research Institute for Smart Energy (RISE)
The Hong Kong Polytechnic University
Kowloon, Hong Kong

of devices being able to withstand 10 000 bending cycles at a radius 0.5 mm.[7] Shelf-life of fPSCs exceeding 1000 h without encapsulation has also been reported,[21,43] which also represents significant achievement in fPSC stability. However, the issue of long term operational stability still remains to be addressed, especially for operational stability in ambient. The stability under illumination has been less commonly reported, and the majority of these studies involved testing under illumination in inert atmosphere.[14,18,20,22,26–28,30,33] Other types of stability tests, such as damp heat test,[40] outdoor testing,[30] and maximum power point (MPP) testing in ambient,[2,12,17,23,35,43,44,46] have been scarce. In the case of illumination in ambient, poor stability has been observed in both inverted (p–i–n) and conventional (n–i–p) architecture fPSCs. For example, the reported T_{80} can be as short as 60 min in inverted fPSCs with commonly used electron transport layer (ETL) 6,6-phenyl-C61-butyric acid methyl ester (PCBM),[2] although longer T_{80} values, such as 81 h, have been reported in devices with PCBM ETL with passivation of hole transport layer (HTL)/perovskite interface.[12] Conventional fPSC have also exhibited poor stability under light soaking in air, with T_{80} less than 1 h,[35] and/or efficiency going to zero after 26 h.[17] While stability of a perovskite solar cell in general (including fPSCs) can be improved by different approaches, such as optimizing the perovskite composition, passivating bulk and interfacial defects, and optimizing device architecture including interfacial and charge transport layers (e.g., using C_{60} instead of PCBM, or inserting inorganic layers),[44,45,49] a significant problem for fPSCs operational stability remains the moisture and oxygen permeability of the flexible polymer substrate. For example, a T_{90} of 150 h in high efficiency flexible tandem devices has been directly attributed to high moisture and oxygen permeability of flexible polymer substrate.[43] While advanced encapsulation, such as the use of glass or barrier foils, could improve operational stability in ambient,[30,34] it is desirable to investigate whether simple modifications of flexible substrates could have a significant effect on device stability as the glass encapsulation is not desirable and ultrahigh barrier foils have relatively high cost.[40] The effect of ultrahigh barrier foils on the shelf-life of perovskite devices has been investigated, but there was no comprehensive investigation of the effect of type of barrier on the stability under illumination.[42]

In general, the inferior operational stability of fPSCs is an intrinsic problem of using flexible plastic substrates, which have significantly higher water vapor transmission ratios (WVTR) and oxygen transmission ratios (OTR)[2,4,6,29,31] compared to rigid glass substrates (WVTR of 10^{-5}–10^{-6} g m^{-2} day^{-1}),[4,6,21] as well as compared to the requirement for barriers for encapsulation of perovskite solar cells (10^{-3}–10^{-6} g m^{-2} day^{-1} for WVTR and 10^{-3}–10^{-6} cm^3 m^{-2} day^{-1} for OTR, respectively).[4,40,50] For example, common polymer substrates, such as polyethylene terephthalate (PET) and polyethylene naphthalate (PEN), typically have WVTR is of the order 10^0–10^2 g m^{-2} day^{-1},[4,6,21,51–53] and OTR of PET and PEN substrates is of the order 10^0–10^1 cc m^{-2} day^{-1}.[51,53] Due to high WVTR and OTR and resulting permeation of moisture and oxygen into fPSCs, poor stability under illumination in ambient occurs. While other possible substrates (metal foils, mica, ultrathin flexible glass)[2] do not suffer from this problem, they have other disadvantages such as not being transparent (metal foils) or having lower bendability and higher

cost (ultrathin glass, mica) and consequently achieving significantly lower record efficiencies compared to devices on polymer substrates.[2,3]

Thus, there is considerable interest in addressing the important disadvantage of polymer substrates, namely high WVTR and OTR. A significant reduction of WVTR by deposition of single layer or multilayer barrier films has been demonstrated for a variety of materials,[4] but the effect of such films on OTR has been less commonly investigated,[51,53] and the effect on fPSC stability is unknown. In general, the efforts to modify the polymer substrate or develop thin film encapsulation frequently involve deposition of hydrophobic layers,[4,37,39,50] which improve the ambient stability in the presence of moisture. In addition to the deposition of thin films on the substrate or top of the device, the use of crosslinking surface modifications for ETL which reduce WVTR have also been demonstrated.[21] Since both moisture and oxygen have the potential to result in perovskite degradation[54–59] and thus negatively affect the performance of fPSCs, it is important to investigate the effects of the deposition of barrier films on OTR and WVTR and resulting device stability. Exposure to moisture causes reversible (formation of hydrated perovskite) and irreversible (deprotonation of organic cation, formation of HI) degradation of the perovskite and contributes to the degradation both in the dark and under illumination,[54] while oxygen-induced degradation is relevant under illumination (photooxidation of the perovskite material).[9,54–57] In addition, while the photooxidative degradation under illumination occurs in the absence of moisture and the presence of oxygen,[9] it can be accelerated by the presence of moisture.[58,59] Thus, both WVTR and OTR of the polymer substrate are expected to affect the stability of devices under illumination.

Therefore, here we investigated the stability of fPSCs under illumination for three different substrate modifications. As the substrate modifications are performed on the back of the substrate, they are not expected to affect device performance provided that they do not reduce the substrate transmittance and that processing of the coating does not alter the properties of PEN substrate. As the devices are encapsulated with polyisobutylene (PIB), commonly used encapsulation material with excellent barrier properties,[50] the main pathway for the moisture/oxygen ingress is expected to be through the substrate and therefore affected by the deposited layers. The encapsulation does not have a significant effect on device efficiency (Figure S1, Supporting Information), and it allows us to selectively study the effect of substrate back-surface modification on stability. Among different modifications investigated, ZnO nanorods modified with fluorinated self-assembled monolayer (1H,1H,2H,2H-perfluorooctyltriethoxysilane (PFOTES)) were selected as surface modification which is expected to have high hydrophobicity based on previous reports on hydrothermally grown ZnO nanorods with surface modifications.[60] Highly hydrophobic modifications are of interest since their deposition the back surface of polymer substrate has a potential advantage of acting as antireflection layer, as well as provide self-cleaning function.[37] In addition, hydrophobic surface modifications are commonly used to improve environmental stability of perovskite films and devices, but at present the effect of hydrophobic modification of flexible substrate on WVTR and device stability is not fully clear. The second modification, spin-coated spin-on-glass layer IC1-200,

was selected due to simple processing, which does not require any additional equipment and can be performed in any lab working on PSCs and commercial spin-on-glass formulations are readily available due to their applications in electronics industry. Finally, the third modification was Al_2O_3 film deposited by atomic layer deposition (ALD). ALD has been previously to directly deposit alumina on top of the perovskite film and thus improve the perovskite stability,[61] but in this work we are mainly interested in using this technique to reduce moisture and oxygen ingress through the substrate. ALD deposition of alumina is particularly promising for reducing WVTR of the polymer substrate,[52] due to dense conformal coating. In addition, WVTR can be maintained over a large number of bending cycles, demonstrating mechanical robustness of ALD-coated barriers.[62] While alumina layers could also be deposited by sputtering, the adhesion of the coating can be strongly dependent on deposition conditions,[63] and generally ALD provides superior coverage of defects/pinholes compared to sputtering.[64] Thus, we will compare the effect of hydrophobic surface modification, low cost solution processed barrier layer, and dense conformally coated barrier on the substrate WVTR and OTR, followed by an investigation of operational stability of fPSCs.

All the selected processes are scalable, and have been used to prepare 10 cm × 10 cm samples for OTR measurements. However, the substrate size for device fabrication is determined by the sample holders (2.5 cm × 2.5 cm), while the device areas are limited by substrate patterns and deposition masks used. In addition, since the investigated barrier layers are insulating (with the exception of ZnO), they have been deposited on the back surface of the substrate. The barrier layers could also be potentially deposited below the indium tin oxide (ITO), but this would require separate optimization of ITO deposition conditions.

In contrast, the modifications of substrate back surface are readily applicable to commercial flexible substrates. The fPSC used for operational stability testing have inverted device architecture with passivated NiO_x/perovskite interfaces, based on our previous work.[12] The T_{80} of the devices under simulated one sun illumination and MPP in ambient could be extended from ≈80 to ≈370 h by deposition of ALD alumina film as thin as ≈10 nm. Solution-processed spin-on glass layer also resulted in a significant increase of T_{80} (≈357 h) compared to devices prepared on substrates without modification. The effects of substrate coating properties on the improvement of device lifetime are discussed.

2. Results and Discussion

Figure 1 shows the contact angles of water on the back surface of PEN/ITO with different surface modifications, and the determined contact angles are summarized in Table S1, Supporting Information. We can observe that IC1-200 does not have a significant effect on the contact angle, alumina film leads to a very small increase, while as expected ZnO/PFOTES coating leads to a significant increase of the contact angle, due to highly hydrophobic PFOTES coating.

The measured OTR and WVTR values are shown in **Figure 2**, and summarized in Table S2 and S3, Supporting Information. Conductivity of Ca film used for WVTR determination is shown in Figure S2, Supporting Information. Ca test is commonly used to determine WVTR,[42,65–67] since the permeation of moisture into the device package will result in the decrease of conductivity of Ca electrodes. The conductivity dependence on time is typically showing a flat region from which lag time is determined, followed by decrease in conductivity from which WVTR is calculated.[42,65–67] It should be noted that the values for
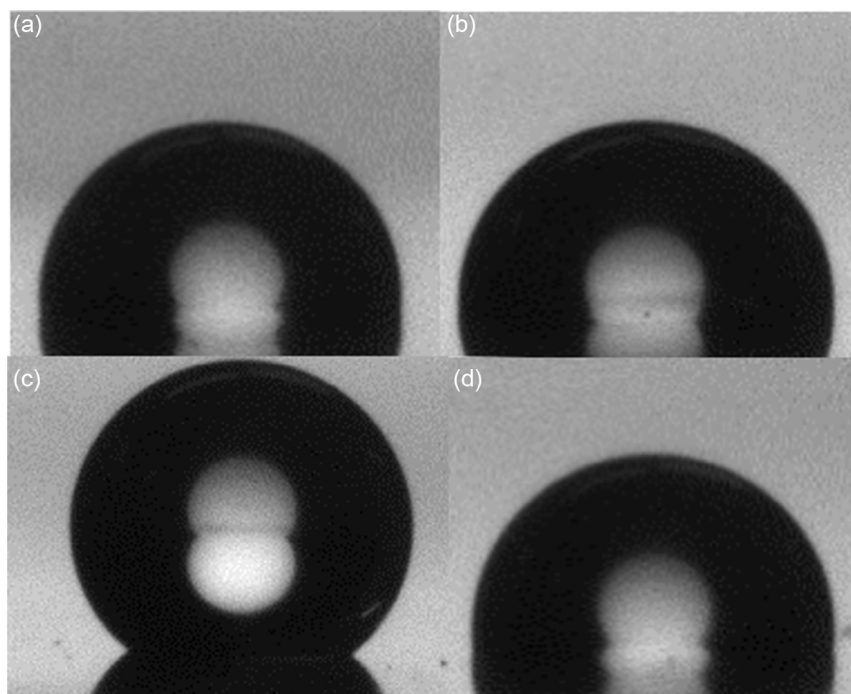
Figure 1. Water droplets on the back surface of PEN/ITO substrates for a) no modifications b) IC1-200 c) ZnO/PFOTES and d) Al_2O_3.
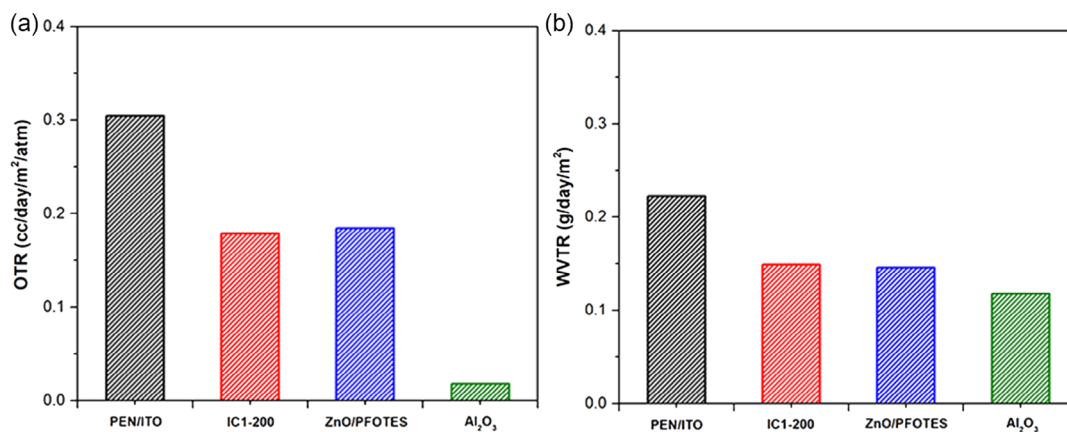
**Figure 2.** a) OTR and b) WVTR of PEN/ITO substrates with different surface modifications.

unmodified substrates are lower compared to reported values for PEN,[41] which is likely due to the presence of ITO film. We can observe that all coatings lead to a decrease in WVTR and OTR, with the lowest values obtained for alumina ALD films, despite their low thickness ($\approx$10 nm). The scanning transmission electron microscopy (STEM) images of the cross-sections of modified substrates are shown in **Figure 3**, while the top view of ZnO nanorods is shown in Figure S3a,b, Supporting Information. We can observe that the thickness of the amorphous IC1-200 layer is $\approx$200 nm, while the length of ZnO nanorods is $\approx$30 nm. The ZnO nanorods exhibit good vertical orientation (Figure S3a,b, Supporting Information).

The transmission of the PEN/ITO substrates with different surface modifications is shown in **Figure 4**a, while the transmission for the same modifications on bare PEN is shown in Figure S4, Supporting Information. We can observe that for bare PEN, $\approx$10 nm alumina film does not result in any significant change in the transmission as expected. PFOTES/ZnO and
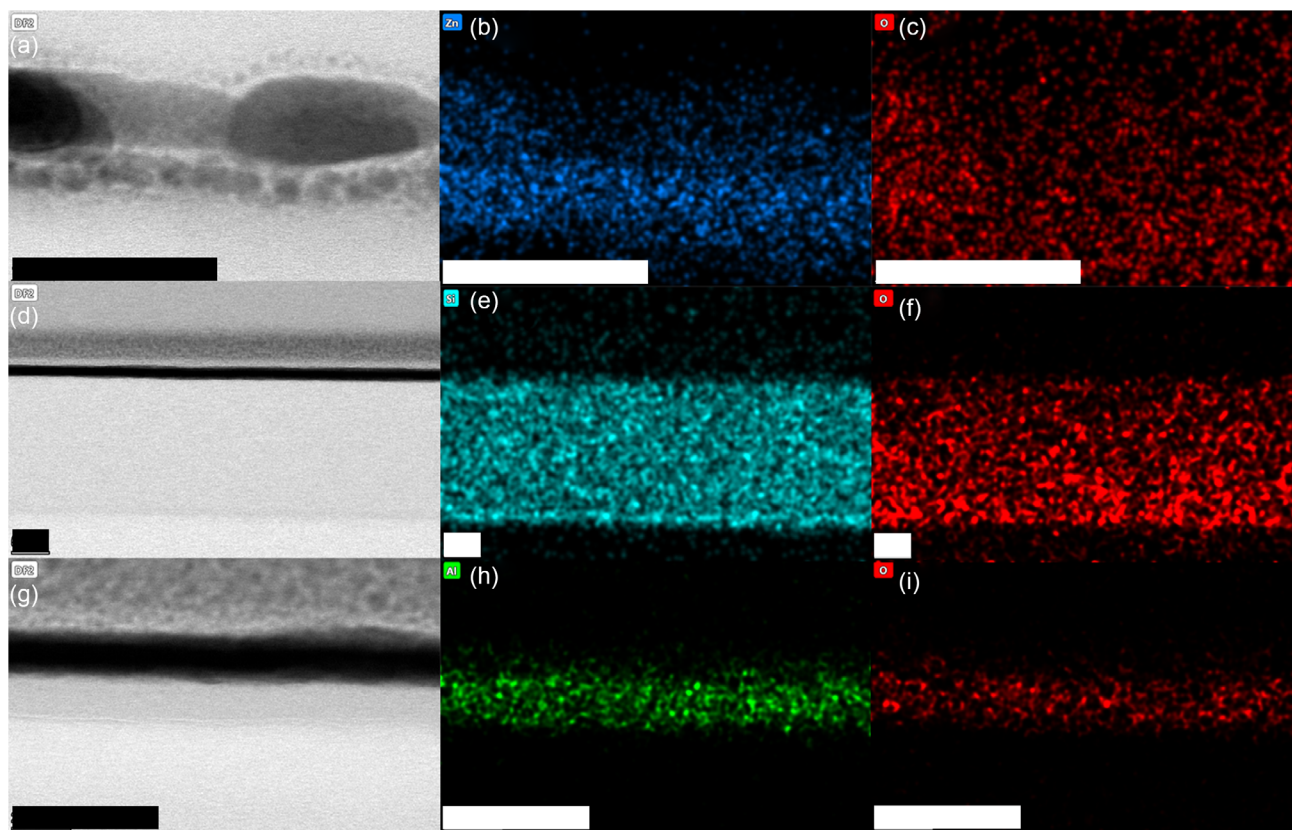
Figure 3. STEM images and EDX mapping for the cross section of a–c) PFOTES/ZnO/PEN d–f) IC1-200/PEN, and g–i) Al$_2$O$_3$/PEN. Scale bar is 50 nm.
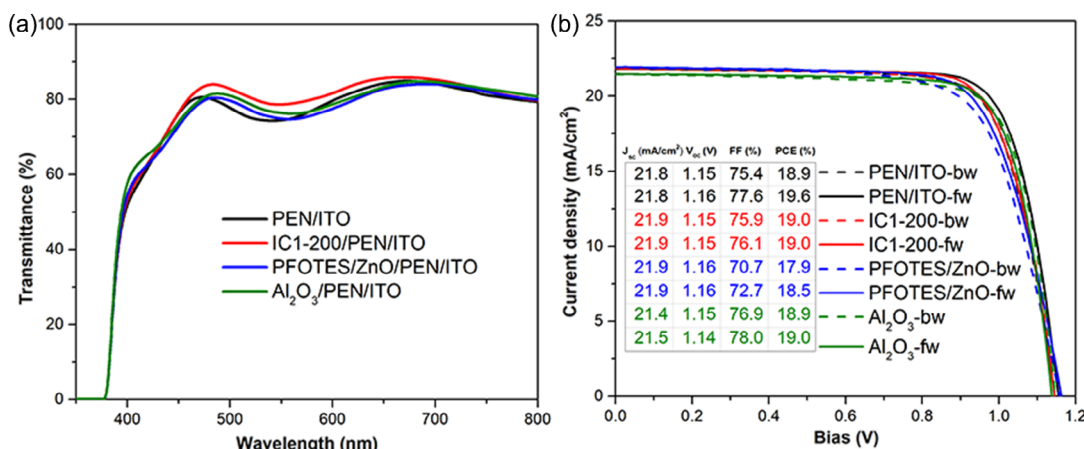
Figure 4. a) Transmission of PEN/ITO with different surface modifications b) I–V curves of fPSCs prepared on substrates with different surface modifications.
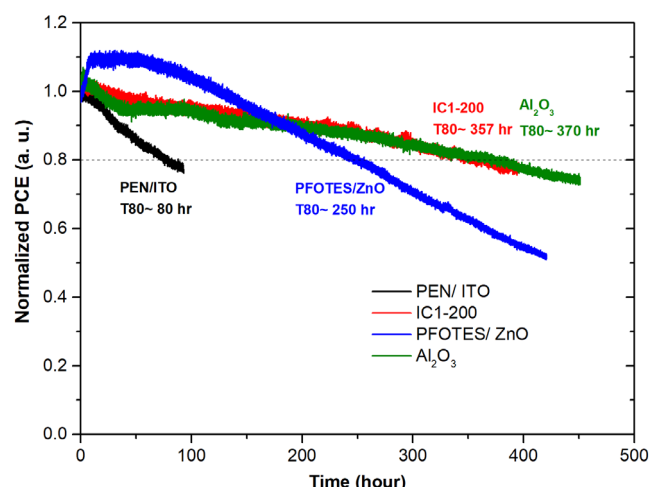
IC1-200 surface modifications result in increased transmittance of PEN in the visible spectral region. In the case of PEN/ITO, we observe some differences compared to bare PEN substrates, which can be attributed to more complex sample structure and interference effects at multiple surfaces in the samples. All the selected barrier materials have wide bandgap, and thus they are not expected to result in increased absorption losses. However, barrier layer thickness can affect the transmission due to interference, in particular for IC1-200 which has thickness values in the range where interference effects in the visible spectral range would be expected. ALD-coated layer is much thinner, and its thickness is limited by deposition time needed, while for ZnO nanorods smaller aspect ratio is preferred due to improved mechanical properties (longer rods are more fragile). Thus, we prepared samples with different spinning speed of IC1-200, and the transmittance of PEN and ITO/PEN for different IC1-200 spinning speed is shown in Figure S5, Supporting Information. We can observe that transmittance of bare PEN is higher for all cases, while for ITO/PEN we can observe increased transmittance in different regions for different spinning speeds, with variations similar to those observed for different coatings. Thus, we do not expect device efficiency to be significantly affected by the IC1-200 spinning speed/thickness, and therefore we will focus on one spinning speed in the middle range of spinning speeds giving good quality films, namely 4000 rpm.

The I–V curves of the fPSCs prepared on substrates with different surface modifications are shown in Figure 4b, while the performance parameters are summarized in Table S4 and S5 and Figure S6, Supporting Information. The performances of all the devices are similar, with the exception of PFOTES/ZnO where a small reduction in the efficiency is observed. All the devices exhibit a small degree of inverted hysteresis (higher efficiency observed under forward compared to reverse scan).[68–70] While hysteresis of J–V curves with higher efficiency observed under reverse scan, both types of hysteresis have been previously observed in both conventional and inverted architectures with different perovskite compositions, and they are generally attributed to the redistribution of mobile ions in the devices.[68–70]

The inverted hysteresis is dependent on ion diffusion rate and ion concentration (quality of perovskite layer), as well as device architecture (the choice of charge transport layers).[68] Devices with NiO_x and PCBM charge transport layers (charge transport layers in this work) in particular were found to exhibit inverted hysteresis over a wide range of scan rates.[68]

The reduction in efficiency for PFOTES/ZnO coating is possibly due to more complex surface modification procedure, where PFOTES modification is performed after the device fabrication to ensure good reproducibility of surface modification properties, since this layer is less mechanically robust and can be damaged during device fabrication. Thus, these devices have additional exposure to higher temperature compared to other devices, which could cause a small reduction in the efficiency. These devices also exhibit worse mechanical stability, as shown in Figure S7, Supporting Information, which would also be expected due to higher processing temperature. Other two substrate modifications, namely ALD alumina and IC1-200, do not have significant effect on device mechanical stability, as expected since all modifications are applied to the back surface of the substrate and thus mechanical damage of the back surface coating, if any, does not affect the device efficiency.

Finally, we examined the stability of fPSCs (schematic diagram of encapsulated devices is shown in Figure S8, Supporting Information) for different substrate modifications, and the obtained results are shown in **Figure 5** (the comparison without normalizing PCE is shown in Figure S9, Supporting Information). We can observe that significant enhancement of the efficiency is obtained for all the surface modifications compared to the PEN/ITO without surface modifications. The obtained T_{80} for fPSCs on unmodified substrates is 80 h, while for PFOTES/ZnO it increases to 250 h, and for IC1-200 and alumina it increases significantly to 357 and 370 h, respectively. The degradation trends follow closely the trends observed in WVTR. The sample with the shortest lag time and highest WVTR among all modifications in PFOTES/ZnO. The lag time can be interpreted as the time needed for water molecules to saturate the substrate and pass through the substrate.[67] Small increase in the lag time for PFOTES/ZnO compared to unmodified

ADVANCED
SCIENCE NEWS
www.advancedsciencenews.com

Energy Technology
Generation, Conversion, Storage, Distribution
www.entechnol.de

Figure 5. Normalized PCE vs. time for fPSCs with different substrate modifications under MPP testing under 1 sun illumination in ambient (60–70% relative humidity) (ISOS-L-1).

substrate is expected as ZnO nanorods do not form a continuous layer on the surface. The lag time is comparable for thicker IC1-200 and very thin alumina layer, due to the fact that ALD deposition typically results in compact and uniform films. These two conditions result in similar T_{80} values, with slightly longer T_{80} obtained for alumina surface modification, which exhibits the lowest OTR and WVTR.

Thus, although both oxygen and moisture contribute to degradation of perovskite under illumination, the diffusion of moisture into the devices through the flexible plastic substrate appears to have more significant effect on the device lifetime. It should be noted that this applies for single layer barriers which do not result in large reductions in WVTR, since it is necessary to use multilayer barriers to reduce WVTR and OTR by several orders of magnitude.[43] Due to complex interplay between oxygen and moisture mediated degradation processes,[55,56] we cannot exclude the possibility that stability under illumination would be more significantly affected by OTR for significantly lower WVTR. Nevertheless, even a small reduction in WVTR

and OTR can result in significant improvement in fPSC lifetime under illumination, clearly demonstrating potential for the operational stability improvement using simple back surface modifications, which could potentially enable elimination of costly ultrahigh barrier foil encapsulation.

To further examine the effect of moisture ingress, we have performed water immersion tests on perovskite films deposited on HTL (so that we could examine degradation of the film due to moisture by X-ray diffraction (XRD) measurements). Obtained results are shown in **Figure 6**. We can observe that for IC1-200 and ALD Al_2O_3 perovskite films stay dark after 72 h immersion in water, and in XRD patterns we only see the relevant perovskite peaks. In contrast, the change of film color to yellow and the appearance of peaks corresponding to PbI_2 and hydrate form of perovskite[71,72] occurs in control samples and samples with ZnO/PFOTES surface modification. This clearly demonstrates that coating the back surface of PEN/ITO with ALD Al_2O_3 or with IC1-200 can effectively inhibit the ingress of moisture through the substrate.

Further improvements are likely by using thicker alumina film (24 nm ALD alumina film could reduce WVTR to the order of magnitude of 10^{-3} g m^{-2} day^{-1}[42]) or by using multilayer barriers. However, not all layer combinations would necessarily be compatible or result in performance improvement. For example, the ZnO nanostructure growth on ALD alumina results in a change in the nanostructure morphology, as shown in Figure S3c,d, Supporting Information, and while the samples are hydrophobic (to a smaller degree compared to nanorods), the T_{80} is not increased compared to single alumina film, as shown in Figure S10, Supporting Information.

3. Conclusion

We have investigated the effect of surface modifications of PEN/ITO substrates on their WVTR and OTR, and consequently on the stability of fPSCs under illumination in ambient for different surface modifications. We have found that significant improvement in stability under illumination is obtained for all surface modifications. The largest improvement, namely an increase in T_{80} under illumination in ambient by 4.6 times
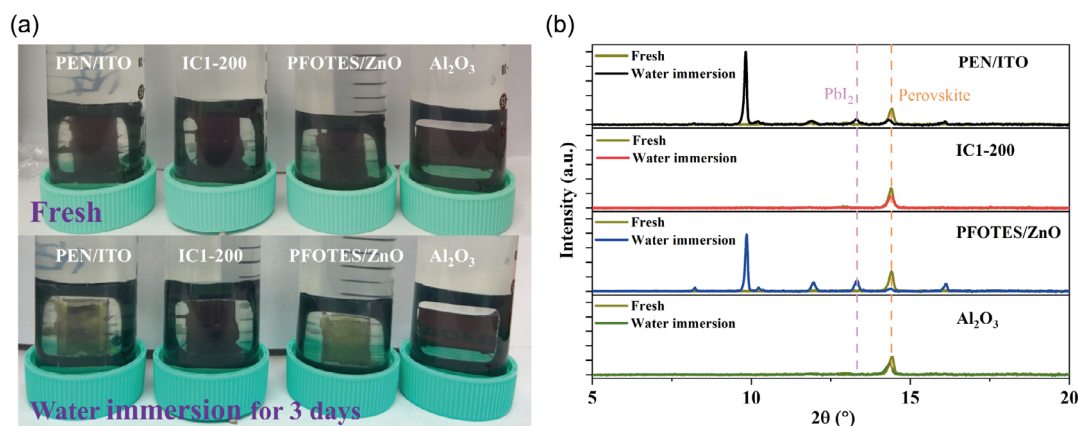
Figure 6. a) Photos and b) XRD patterns of perovskite sub-cells on substrates with different surface modifications.

compared to unmodified substrates is obtained by deposition of very thin ($\approx$10 nm) alumina coating on the back surface of PEN/ITO. Comparable improvement ($\approx$4.5 times increase in T_{80}) is obtained for solution processed spin-on-glass as a barrier layer, demonstrating potential for simple modifications of back surface of the PEN/ITO substrates to significantly improve operational stability.

4. Experimental Section

Materials: PEN/ITO substrates were obtained from Peccell. Zinc acetate, hexamethylenetetramine, polyethyleneimine (PEI, 50 wt% in water), zinc nitrate hexahydrate, methanol, and 1H, 1H, 2H, 2H-perfluorooctyltriethoxysilane (PFOTES) were purchased from Sigma Aldrich. Ethanolamine, [2-(9H-carbazol-9-yl)ethyl]phosphonic acid (2PACz), lead bromide (PbBr$_2$), and lead iodide (PbI$_2$) were obtained from TCI. Formamidinium iodide (FAI), phenethylammonium iodide (PEAI), and methylammonium bromide (MABr) were purchased from Great Cell Solar. Bathocuproine (BCP) and (6,6)-phenyl C$_{61}$ butyric acid methyl ester (PCBM) were purchased from Lumtec. Cesium iodide (CsI), N, N-Dimethylformamide (DMF), dimethyl sulfoxide (DMSO), and isopropanol (IPA) were purchased from Alfa Aesar. Chlorobenzene (CB) was obtained from Aladdin, while ethanol was purchased from Anaqua. Trimethylaluminum (TMAl) was obtained from FornAna, IC1-200 was obtained from Futurrex, and calcium was purchased from ZhongNuo Advanced Material Co. Ltd. NiO$_x$ nanoparticles ink (20 mg mL^{-1} in DI water) was prepared as reported previously. All materials were used as received, without further purification.

Substrate Modification: PEN/ITO substrates were sonicated in detergent (Decon 90), DI water, and ethanol sequentially for 15 min each, and then blow-dried with N$_2$. The substrate surface was then treated with O$_2$ Plasma at 10 V for 10 s before substrate modification or PSCs fabrication. For IC1-200 modification, IC1-200 solution was spin coated onto cleaned PEN surface at a specific spinning speed (4000 rpm unless specified otherwise) for 30 s, followed by annealing at 110 °C for 1 h. Alumina (Al$_2$O$_3$) coating was deposited using ALD. The Al source and O source were Trimethylaluminum (TMAl) and DI water, respectively. The cleaned PEN/ITO substrate was transferred into ALD chamber, and deposition was performed at 150 °C and $\approx$2 × 10^{-1} torr. PEN/ITO substrates were placed on glass slide with ITO side face down and PEN side exposed to ALD reaction chamber. To protect ITO side from Al$_2$O$_3$ deposition, the substrate edge was sealed to the glass slide by Kapton tape. N$_2$ was used as a carrier gas, at a flow rate of 20 sccm. One ALD cycle consisted of Al precursor pulse of 0.0025 s, followed by 15 s N$_2$ purge, and DI water pulse for 0.02 s, followed by N$_2$ purge for 15 s. For each cycle, about 1.6 Å of Al$_2$O$_3$ was deposited, and the total number of cycles was 60. We also considered surface-modified ZnO nanorods as a coating. To grow ZnO nanorods, ZnO seed layer was deposited first by via spin-coating solgel solution. The solution was prepared by dissolving zinc acetate in ethanol (40 mg mL^{-1}) and adding ethanolamine (20 µL mL^{-1}), followed by stirring at 80 °C for 1 h, and filtering by a PTFE filter before use. As-prepared solution was spin-coated on the back surface of PEN at 4000 rpm for 30 s, followed by annealing at 110 °C for 1 h. The solution for ZnO nanorod growth was prepared by dissolving 0.1 g of polyethyleneimine, 0.56 g of zinc nitrate hexahydrate, and 0.26 g of hexamethylenetetramine in 75 mL of DI water with vigorous stirring. The substrates with ZnO seed layer were placed in contact with the solution in an oven at 90 °C for 20 min with ITO side protected to prevent ZnO nanorod growth. ZnO nanosheet growth on as prepared alumina surface following the same procedure. To achieve high hydrophobicity, the surface of ZnO nanorods was modified by spin-coating 1H,1H,2H,2H-Perfluorooctyltriethoxysilane (PFOTES) in ethanol (1:20 v:v) at 1500 rpm for 30 s, followed by annealing at 110 °C for 15 min. The procedure was repeated 3 times for better coverage. PFOTES modification was performed after device fabrication, while other substrate modifications were performed before the device fabrication.

Device Fabrication: Perovskite devices have been prepared as previously described.[12] Briefly, NiO$_x$ ink was spin-coated at 3000 rpm on cleaned substrates and annealed at 110 °C for 10 min. Then, ethanolamine in ethanol (1:50 v:v with ethanol) solution was spin-coated onto NiO$_x$ thin film at 4000 rpm and annealed at 100 °C for 5 min. Then the substrates were transferred into the glovebox and 2PACz was spin-coated at 4000 rpm, followed by annealing at 100 °C for 10 min. The perovskite Cs$_{0.05}$(FA$_{0.85}$MA$_{0.15}$)$_{0.95}$Pb(I$_{0.85}$Br$_{0.15}$)$_3$ was prepared by dissolving mixed powders of 18.2 mg of CsI, 172 mg of FAI, 22.4 mg MABr, 73.4 mg PbBr$_2$, and 507.1 mg of PbI$_2$ in 1 mL of DMF: DMSO (4:1 v:v). The prepared solution was stirred at 65 °C for 2 h. CsFAMA perovskite was then deposited via spin coating at 4000 rpm for 35 s, and at 10 s, 300 µL CB antisolvent was dropped onto the substrate. The CsFAMA perovskite was annealed at 110 °C for 40 min. 2D perovskite was prepared by dynamic spincoating of 1 mg mL^{-1} PEAI solution in IPA onto the perovskite top surface at 5000 rpm, followed by annealing at 100 °C for 3 min. PCBM (20 mg mL^{-1} in CB) ETL was spin coated at 1200 rpm for 30 s, followed by annealing at 100 °C for 10 min. BCP interlayer was spin-coated at 4000 rpm without further annealing. Finally, 100 nm Ag electrode was deposited through a shadow mask via thermal evaporation.

Characterization: J–V scans were measured by the Keithley 2400 source meter under calibrated 1 sun AM 1.5 illumination using ABET Sun 2000 solar simulator. Stability testing was performed in ambient (relative humidity 60–70%) under bias at MPP and illumination at 1 sun intensity (100 mW cm^{-2}) provided by Newport (formerly Oriel) 66 902 solar simulator. External quantum efficiency (EQE) measurements were also performed using Enli QE-R 3011 EQE system, and integrated short circuit current density was determined, as shown in Figure S11 and S12, Supporting Information. Stability tests and I–V curve measurements were performed in air on samples encapsulated using polyisobutylene (PIB) tape and PET cover following ISOS-L-1 testing protocol.[73] Due to the barrier properties of PIB,[50] main pathway for moisture and oxygen ingress was through PEN/ITO substrate. Mechanical stability tests were conducted with a homemade mechanical bending machine, with bending radius of 5 mm. Water immersion test were conducted on PEN/ITO/NiO$_x$-amine/2PACz/perovskite sub-cells with different back surface modifications of PEN in order to characterize the perovskite film by XRD measurements (Rigaku MiniFlex600 with Cu Kα X-ray source) before and after water immersion. After initial XRD measurement, sub cells were encapsulated by PIB edge seal and cover glass. After 72 h of water immersion, the encapsulation was removed and XRD measurement was performed.

SEM was performed using a FEI Nova nanoSem450 SEM. Transmittance spectra were measured using a PerkinElmer LAMBDA 750 s and HITACHI U-2900 spectrometer. Contact angle images were obtained with Krüss Scientific drop shape analyzer DSA25. To obtain WVTR, 300 nm of Ca metal was deposited on patterned ITO via thermal evaporation in thermal evaporator integrated with a glove box. Then, the Ca metal was encapsulated with PIB tape inside the glove box. The encapsulated devices were then transferred to ambient environment. Due to water transmission, Ca metal reacts with H$_2$O and produces insulating Ca(OH)$_2$. The WVTR can be calculated as follows[50–52]:

$$WVTR = -2\left(\frac{M_{H_2O}}{M_{Ca}}\right)\delta\rho\frac{l}{w}\frac{d(\frac{1}{R})}{dt} \qquad (1)$$

where R is the resistance of Ca metal, M$_{H20}$ and M$_{Ca}$ are the molecular weight of H$_2$O (18) and Ca (40) respectively, δ is the density of Ca (1.55 × 10^6 g m^{-3}), ρ is the resistivity of Ca (8.95 × 10^{-8} Ωm), and l and w are the length and width of deposited Ca (10 and 1 mm, respectively). OTR measurements were provided by Beijing ZKGX Research Institute of Chemical Technology. The test samples for OTR measurements were performed on 10 × 10 cm according to test method ASTM D-3985. STEM cross-section samples were prepared with focused ion beam (FIB) FEI Helios Nanolab 600i. STEM-EDX (EDC denotes energy dispersive X-ray spectroscopy) was performed by Titan Themis G2.

Supporting Information

Supporting Information is available from the Wiley Online Library or from the author.

Conflict of Interest

The authors declare no conflict of interest.

Author Contributions

A.M.C.N. and A.B.D. conceived the idea, designed the experiments, and supervised the project. J.Y.L. prepared and characterized the solar cells with the assistance from H.B.M., Y.L., and Z.L.R. assisted with stability measurements. Y.L.H. performed transmittance measurements and STEM imaging. Y.N.C. and J.Y.T. were responsible for ALD deposition, while W.T.W. and S.P.F. contributed to contact angle measurement. A.K. synthesized NiO_x nanoparticles. Z.S. and W.D.L. contributed to mechanical stability characterization, while T.Z. and G.L. provided EQE measurements. A.B.D. prepared the first draft of the manuscript. All authors discussed and analyzed the results and provided input to the manuscript.

Data Availability Statement

The data that support the findings of this study are available from the corresponding author upon reasonable request.

Keywords

flexible perovskite solar cells, solar cell stability, thin film barrier coatings

[1] G. S. Han, H. S. Jung, N. G. Park, *Chem. Commun.* **2021**, *57*, 11604.

[2] S. Mishra, S. Ghosh, T. Singh, *ChemSusChem* **2021**, *14*, 512.

[3] G. Q. Tang, F. Yan, *Nano Today* **2021**, *39*, 101155.

[4] L. J. Sutherland, H. C. Weerasinghe, G. P. Simon, *Adv. Energy Mater.* **2021**, *11*, 2101383.

[5] J. Panidi, D. Georgiadou, T. Schoetz, T. Prodromakis, *Adv. Funct. Mater.* **2022**, *32*, 2200694.

[6] Y. M. Xu, Z. H. Lin, J. C. Zhang, Y. Hao, J. Y. Ouyang, S. Z. Liu, J. J. Chang, *Appl. Phys. Rev.* **2022**, *9*, 021307.

[7] Y. J. Gao, K. Q. Huang, C. Y. Long, Y. Ding, J. H. Chang, D. Zhang, L. Etgar, M. Z. Liu, J. Zhang, J. L. Yang, *ACS Energy Lett.* **2022**, *7*, 1412.

[8] S. Chander, S. K. Tripathi, *Mater. Adv.* **2022**, *3*, 7198.

[9] G. Nazir, S. Y. Lee, J. H. Lee, A. Rehman, J. K. Lee, S. I. Seok, S. J. Park, *Adv. Mater.* **2022**, *34*, 2204380.

[10] Y. Z. Ma, Z. Lu, X. D. Su, G. F. Zou, Q. Zhao, *Adv. Energy Sustainability Res.* **2023**, *4*, 2200133.

[11] Y. M. Xu, Z. H. Lin, W. Wei, Y. Hao, S. Z. Liu, J. Y. Ouyang, J. J. Chang, *Nano-Micro Lett.* **2022**, *14*, 117.

[12] J. Y. Lin, Y. T. Wang, A. Khaleed, A. A. Syed, Y. L. He, C. C. S. Chan, Y. Li, K. Liu, G. Li, K. S. Wong, J. Popović, J. Fan, A. M. C. Ng, A. B. Djurišić, *ACS Appl. Mater. Interfaces* **2023**, *15*, 24437.

[13] X. T. Yin, P. Chen, M. D. Que, Y. L. Xing, W. X. Que, C. M. Niu, J. Y. Shao, *ACS Nano* **2016**, *10*, 3630.

[14] Q. Luo, H. Ma, F. Hao, Q. Z. Hou, J. Ren, L. L. Wu, Z. B. Yao, Y. Zhou, N. Wang, K. L. Jiang, H. Lin, Z. H. Guo, *Adv. Funct. Mater.* **2017**, *27*, 1703068.

[15] X. T. Hu, X. C. Meng, L. Zhang, Y. Y. Zhang, Z. R. Cai, Z. Q. Huang, M. Su, Y. Wang, M. Z. Li, F. Y. Li, X. Yao, F. Y. Wang, W. Ma, Y. W. Chen, Y. L. Song, *Joule* **2019**, *3*, 2205.

[16] J. Y. Lam, J. Y. Chen, P. C. Tsai, Y. T. Hsieh, C. C. Chueh, S. H. Tung, W. C. Chen, *RSC Adv.* **2017**, *7*, 54361.

[17] P. Kumar, A. K. Chauhan, *J. Phys. D: Appl. Phys.* **2020**, *53*, 035101.

[18] G. J. Jeong, D. H. Koo, J. H. Seo, S. G. Jung, Y. S. Choi, J. H. Lee, H. S. Park, *Nano Lett.* **2020**, *20*, 3718.

[19] C. Y. Long, K. Q. Huang, J. H. Chang, C. T. Zuo, Y. J. Gao, X. Luo, B. Liu, H. P. Xie, Z. H. Chen, J. He, H. Huang, Y. L. Gao, L. M. Ding, J. L. Yang, *Small* **2021**, *17*, 2102368.

[20] C. D. Ge, Z. Q. Yang, X. T. Liu, Y. L. Song, A. R. Wang, Q. F. Dong, *CCS Chem.* **2020**, *2*, 2035.

[21] N. Y. Ren, B. B. Chen, R. J. Li, P. Y. Wang, S. Mazumdar, B. Shi, C. J. Zhu, Y. Zhao, X. D. Zhang, *Sol. RRL* **2021**, *5*, 2000795.

[22] Q. S. Dong, M. Chen, Y. H. Liu, F. T. Eickemeyer, W. D. Zhao, Z. H. Dai, Y. F. Yin, C. Jiang, J. S. Feng, S. Y. Jin, S. Liu, S. M. Zakeeruddin, M. Grätzel, N. P. Padture, Y. T. Shi, *Joule* **2021**, *5*, 1587.

[23] L. A. Castriotta, R. F. Pineda, V. Babu, P. Spinelli, B. Taheri, F. Matteocci, F. Brunetti, K. Wojciechowski, A. Di Carlo, *ACS Appl. Mater. Interfaces* **2021**, *13*, 29576.

[24] Y. Tan, B. Xiao, P. Xu, Y. B. Luo, Q. H. Jiang, J. Y. Yang, *ACS Appl. Mater. Interfaces* **2021**, *13*, 20034.

[25] L. Yang, J. S. Feng, Z. K. Liu, Y. W. Duan, S. Zhan, S. M. Yang, K. He, Y. Li, Y. W. Zhou, N. Y. Yuan, J. N. Ding, S. Liu, *Adv. Mater.* **2022**, *34*, 2201681.

[26] Z. H. Zheng, F. M. Li, J. Gong, Y. Y. Ma, J. W. Gu, X. C. Liu, S. H. Chen, M. Z. Liu, *Adv. Mater.* **2022**, *34*, 2109879.

[27] C. H. Chen, Z. H. Su, Y. H. Lou, Y. J. Yu, K. L. Wang, G. L. Liu, Y. R. Shi, J. Chen, J. J. Cao, L. Zhang, X. Y. Gao, Z. K. Wang, *Adv. Mater.* **2022**, *34*, 2200320.

[28] Z. J. Yi, B. Xiao, X. Li, Y. B. Luo, Q. H. Jiang, J. Y. Yang, *J. Colloid Interface Sci.* **2022**, *628*, 696.

[29] J. F. Benitez-Rodriguez, D. H. Chen, A. D. Scully, C. D. Easton, D. Vak, H. Li, P. E. Shaw, P. L. Burn, R. A. Caruso, M. Gao, *Sol. Energy Mater. Sol. Cells* **2022**, *246*, 111884.

[30] V. Babu, M. A. M. Escobar, R. F. Pineda, M. Ścigaj, P. Spinelli, K. Wojciechowski, *Mater. Today Energy* **2022**, *28*, 101073.

[31] Z. Y. Xu, Q. X. Zhuang, Y. Q. Zhou, S. R. Lu, X. H. Wang, W. S. Cai, Z. G. Zang, *Small Struct.* **2023**, *4*, 2200338.

[32] J. Yang, W. P. Sheng, X. Li, Y. Zhong, Y. Su, L. C. Tan, Y. W. Chen, *Adv. Funct. Mater.* **2023**, *16*, 2214984.

[33] J. Dou, Q. Z. Song, Y. Ma, H. Wang, G. Z. Yuan, X. Y. Wei, X. X. Niu, S. Ma, X. Y. Yang, J. Dou, S. C. Liu, H. P. Zhou, C. Zhu, Y. H. Chen, Y. J. Li, Y. Bai, Q. Chen, *J. Energy Chem.* **2023**, *76*, 288.

[34] M. Park, S. C. Hong, Y. W. Jang, J. Byeon, J. Jang, M. Han, U. Kim, K. Jeong, M. Choi, G. Lee, *Int. J. Precis. Eng. Manuf. Green Technol.* **2023**, *10*, 1223.

[35] G. Lucarelli, F. De Rossi, B. Taheri, T. M. Brown, F. Brunetti, *Energy Technol.* **2022**, *10*, 2200314.

[36] Z. Yi, X. Li, B. Xiao, Y. B. Luo, Q. H. Jiang, J. Y. Yang, *Sci. China Mater.* **2022**, *65*, 3392.

[37] E. Cho, Y. Y. Kim, D. S. Ham, J. H. Lee, J. S. Park, J. Seo, S. J. Lee, *Nano Energy* **2021**, *82*, 105737.

[38] H. C. Weerasinghe, Y. Dkhissi, A. D. Scully, R. A. Caruso, Y. B. Cheng, *Nano Energy* **2015**, *18*, 118.

[39] J. Kim, J. H. Jang, J. H. Kim, K. Park, J. S. Jang, J. Park, N. Park, *ACS Appl. Energy Mater.* **2020**, *3*, 9257.

[40] T. Ahmad, S. Dasgupta, S. Almosni, A. Dudkowiak, K. Wojciechowski, *Energy Environ. Mater.* **2023**, *6*, e12434.

[41] Y. Cao, J. Feng, Z. Xu, L. Zhang, J. Lou, Y. Liu, X. Ren, D. Yang, S. F. Liu, *InfoMat* **2023**, *5*, e12423.

[42] S. Castro-Hermosa, M. Top, J. Dagar, J. Fahlteich, T. M. Brown, *Adv. Electron. Mater.* **2019**, *5*, 1800978..

[43] L. Li, Y. Wang, X. Wang, R. Lin, X. Luo, Z. Liu, K. Zhou, S. Xiong, Q. Bao, G. Chen, Y. Tian, Y. Deng, K. Xiao, J. Wu, M. I. Saidaminov, H. Lin, C. Q. Ma, Z. Zhao, Y. Wu, L. Zhang, H. Tan, *Nat. Energy* **2022**, *7*, 708.

[44] L. Xie, S. Y. Du, J. Li, C. Liu, Z. W. Pu, X. Y. Tong, J. Liu, Y. Wang, Y. Meng, M. Yang, W. Li, Z. Ge, *Energy Environ. Sci.* **2023**, *16*, 5423.

[45] D. Gao, B. Li, Z. Li, X. Wu, S. Zhang, D. Zhao, X. Jiang, C. Zhang, Y. Wang, Z. Li, N. Li, S. Xiao, W. C. H. Choy, A. K. Y. Jen, S. Yang, Z. Zhu, *Adv. Mater.* **2023**, *35*, 2206387..

[46] M. Karimipour, S. Khazraei, B. J. Kim, G. Boschloo, E. M. J. Johansson, *Nano Energy* **2022**, *95*, 107044..

[47] Z. Yi, B. Xiao, X. Li, Y. Luo, Q. Jiang, J. Yang, *Nano Energy* **2023**, *109*, 108241..

[48] Z. Yi, X. Li, B. Xiao, Q. Jiang, Y. Luo, J. Yang, *Chem. Eng. J.* **2023**, *469*, 143790..

[49] X. Li, G. Shen, X. R. Ng, Z. Liu, Y. Meng, Y. W. Zhang, C. Mu, Z. G. Yu, F. Lin, *Energy Environ. Mater.* **2022**, *6*, e12439..

[50] Y. T. Wang, I. Ahmad, T. L. Leung, J. Y. Lin, W. Chen, F. Z. Liu, A. M. C. Ng, Y. Zhang, A. B. Djurišić, *ACS Mater. Au* **2022**, *2*, 215.

[51] H. N. Ra, S. S. Kim, *Mol. Cryst. Liq. Cryst.* **2012**, *564*, 138.

[52] K. L. Jarvis, P. J. Evans, G. Triani, *Surf. Coat. Technol.* **2018**, *337*, 44.

[53] S. G. Kim, N. H. You, B. C. Ku, H. S. Lee, *ACS Appl. Nano Mater.* **2020**, *3*, 8972.

[54] C. C. Boyd, R. R. Cheacharoen, T. Leijtens, M. D. McGehee, *Chem. Rev.* **2019**, *119*, 3418.

[55] N. Aristidou, C. Eames, I. Sanchez-Molina, X. N. Bu, J. Kosco, M. S. Islam, S. A. Haque, *Nat. Commun.* **2017**, *8*, 15218.

[56] G. Abdelmageed, L. Jewell, K. Hellier, L. Seymour, B. B. Luo, F. Bridges, J. Z. Zhang, S. Carter, *Appl. Phys. Lett.* **2016**, *109*, 233905.

[57] N. Aristidou, I. Sanchez-Molina, T. Chotchuangchutchaval, M. Brown, L. Martinez, T. Rath, S. A. Haque, *Angew. Chem., Int. Ed.* **2015**, *54*, 8208.

[58] Y. Ouyang, L. Shi, Q. Li, J. Wang, *Small Methods* **2019**, *3*, 1900154.

[59] T. D. Siegler, W. A. Dunlap-Shohl, Y. Meng, Y. Yang, W. F. Kau, P. P. Sunkari, C. E. Tsai, Z. J. Armstrong, Y. C. Chen, D. A. C. Beck, M. Meilâ, H. W. Hillhouse, *J. Am. Chem. Soc.* **2022**, *144*, 5552.

[60] R. S. Sabry, N. K. Fahad, *J. Adhes. Sci. Technol.* **2019**, *33*, 1558.

[61] J. Gong, M. Adnani, B. T. Jones, Y. Xin, S. Wang, S. V. Patel, E. Lochner, H. Mattoussi, Y. Y. Hu, H. Gao, *J. Phys. Chem. Lett.* **2022**, *13*, 4082.

[62] J. H. Woo, D. H. Koo, N. H. Kim, H. Kim, M. H. Song, H. Park, J. Y. Kim, *ACS Appl. Mater. Interfaces* **2021**, *13*, 46894.

[63] R. Cueff, G. Baud, M. Benmalek, J. P. Besse, J. R. Butruille, H. M. Dunlop, M. Jacquet, *Thin Solid Films* **1995**, *270*, 230.

[64] U. S. Lee, J. S. Choi, B. S. Yang, S. Oh, Y. J. Kim, M. S. Oh, J. Heo, H. J. Kim, *ECS Solid State Lett.* **2013**, *2*, R13.

[65] S. Y. Zhang, Y. Xue, Z. N. Yu, *Thin Solid Films* **2015**, *580*, 101.

[66] S. J. Kim, T. Y. Kim, B. H. Kang, G. H. Lee, B. K. Ju, *RSC Adv.* **2018**, *8*, 39083.

[67] J. A. Bertrand, D. J. Higgs, M. J. Young, S. M. George, *J. Phys. Chem. A* **2013**, *117*, 12026.

[68] R. García-Rodríguez, A. J. Riquelme, M. Cowley, K. Valadez-Villalobos, G. Oskam, L. J. Bennett, M. J. Wolf, L. Contreras-Bernal, P. J. Cameron, A. B. Walker, J. A. Anta, *Energy Technol.* **2022**, *10*, 2200507.

[69] D. A. Jacobs, Y. Wu, H. Shen, C. Barugkin, F. J. Beck, T. P. White, K. Weber, K. R. Catchpole, *Phys. Chem. Chem. Phys.* **2017**, *19*, 3094.

[70] W. Tress, J. P. Correa Baena, M. Saliba, A. Abate, M. Graetzel, *Adv. Energy Mater.* **2016**, *6*, 1600396.

[71] R. Segovia, G. Qu, M. Peng, X. Sun, H. Shi, B. Gao, *Nanoscale Res. Lett.* **2018**, *13*, 79.

[72] A. M. A. Leguy, Y. Hu, M. Campoy-Quiles, M. I. Alonso, O. J. Weber, P. Azarhoosh, M. van Schilfgaarde, M. T. Weller, T. Bein, J. Nelson, P. Docampo, P. R. F. Barnes, *Chem. Mater.* **2015**, *27*, 3397.

[73] M. V. Khenkin, E. A. Katz, A. Abate, G. Bardizza, J. J. Berry, C. Brabec, F. Brunetti, V. Bulović, Q. Burlingame, A. Di Carlo, R. Cheacharoen, Y. B. Cheng, A. Colsmann, S. Cros, K. Domanski, M. Dusza, C. J. Fell, S. R. Forrest, Y. Galagan, D. Di Girolamo, M. Grätzel, A. Hagfeldt, E. Von Hauff, H. Hoppe, J. Kettle, H. Köbler, M. S. Leite, S. Frank Liu, Y. L. Loo, J. M. Luther, *et al.*, *Nat. Energy* **2020**, *5*, 35.